PERGAMON

Computers & Fluids 28 (1999) 19–39

computers & fluids

A finite element study of the blood flow in total cavopulmonary connection

T.W.H. Sheu[a,*], S.F. Tsai[a], W.S. Hwang[a], T.M. Chang[b]

[a]*Department of Naval Architecture and Ocean Engineering, National Taiwan University, 73 Chou-Shan Road, Taipei, Taiwan, Republic of China*

[b]*Buddhist Tzu Chi General Hospital, 707, Section 3, Chung-yang Rd, Hualien, Taiwan, Republic of China*

Received 9 June 1997; received in revised form 2 April 1998

Abstract

The present study is a preliminary investigation into the total cavopulmonary connection (TCPC) blood flow structure in Fontan procedures. Our aim is to gain a better understanding of flow reversal in vascular circulation. In this paper we consider a two-dimensional mathematical model of the Navier–Stokes equations. Specifically, we study the laminar flow in the blood vessel with outlets at which a free boundary condition is specified. To further simplify the analysis, the vessel walls are regarded as being rigid. In quadratic elements, we employ the streamline upwind Petrov–Galerkin finite element model as our strategy to simulate incompressible fluid flows. The adopted finite element model is featured by the presence of artificial damping terms added solely in the streamline direction. With these terms added to the formulation, the discrete system is enhanced while solution accuracy is maintained without deterioration due to false diffusion errors. In this finite element flow study, our emphasis is placed on the role of the offsets as a control parameter in order to optimize the blood flow after the surgical intervene.

1. Introduction

Depending on physiologic conditions and organ demands, blood vessels in the human vascular system serve to supply human organs with their required amounts of blood. Under normal conditions [Fig. 1(a)], arteries can adapt to changes in blood flow and blood pressure. However, under certain abnormal circumstances [Fig. 1(b)], defects in the vascular system cause arteries to fail to respond to imposed forces and, in the worst case, to be unable to provide adequate blood to important organs. According to Kim et al. [1], 7 out of 1000 babies

* To whom correspondence should be addressed.

0045-7930/99/$ - see front matter
PII: S0045-7930(98)00018-8

have congenital heart defects, resulting in impairment of the flow of unoxygenated blood to the lungs. To fix this problem, the Fontan procedure [2] emerges as a surgical means to correct such heart defects. The idea behind Fontan procedures is to reroute the blood flow around these congenital passage blocks, thus allowing the blood to reach the lungs. Depending on surgical techniques, there exist three main classes of Fontan circulation procedures. They are the atriopulmonary connection (APC), cavopulmonary connection (CPC), and bidirectional cavopulmonary anastomosis (BCPA). Previous studies showed that the hemodynamic and energetic differences between different connections are small. Such small differences, however, play a crucial role in the determination of failure or success of long-term follow-up patients who have undergone Fontan operations [3]. This observation shows the need to perform a detailed study to gain insight into the hemodynamics in vascular circulation.

In this study, we consider the total cavopulmonary connection (TCPC), which is a clinical operation specifically designed for surgery on hearts with essentially a single ventricular chamber [4, 5]. As Fig. 1 shows, the TCPC operation involves disconnection of the pulmonary artery from its ventricular origin, together with anastomosis of the superior vena cava (SVC)

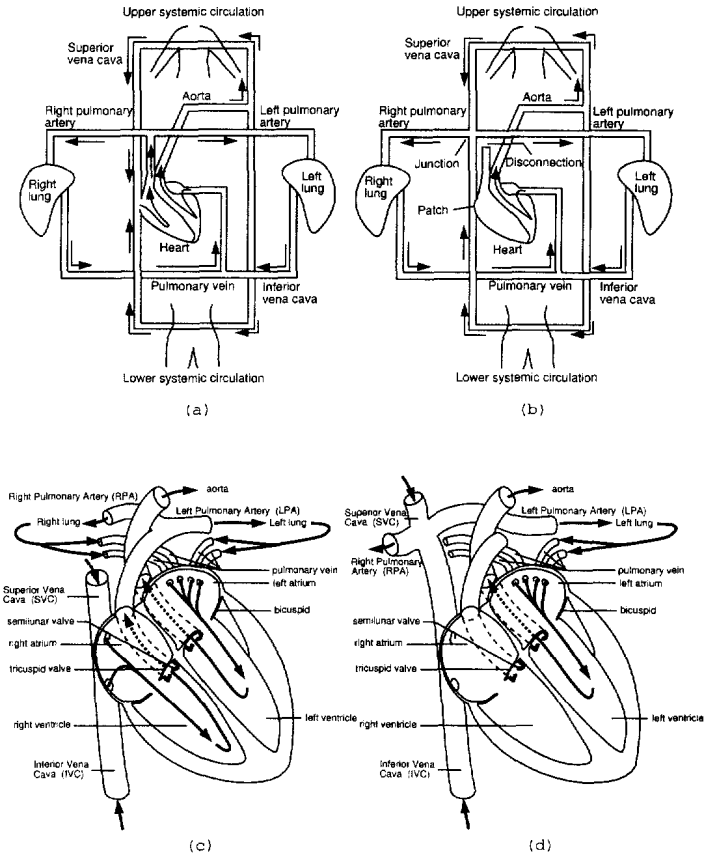

Fig. 1. (a) The principal blood circulation system for a normal human being; (b) the principal blood circulation system after the TCPC operation; (c) a schematic drawing of anatomy of normal vascular circulation system; (d) illustration of anatomy after the TCPC anastomosis.

with the right pulmonary artery. The operation is completed with construction of a right atrial lateral tunnel. The tunnel connects the inferior vena cava (IVC) to the transected end of the SVC, which is anastomosed to the right and main pulmonary artery. Completion of the TCPC operation results in a by-pass of the right heart with the ability to create circulation driven solely by a single ventricular pump [Fig. 1(d)]. Given that the energy generated by the left ventricular pump is mostly dissipated in the systemic circulation the fluid dynamics in the venae cavae and the pulmonary circulation are particularly precarious. Due to this potential loss of steadiness, the operation warrants a detailed pre-study to yield good hemodynamics in the anastomotic region.

A long-term success of a TCPC operation can be assessed from many aspects. From the fluid dynamics viewpoint, a surgically created circuit serves to avoid vortices, separation, recirculation, and stagnation in the blood flow. These abnormalities may induce low shear stress and oscillating in pulsatile situations. This, in turn, could induce atherosclerosis and cause increased energy dissipation in the blood flow. Also, high shear stresses are not permitted since they tend to damage the blood vessel. From the energy point of view, surgically created monoventricular circulation should provide adequate pulmonary perfusion for the global circulatory system. In fluid dynamic terms, proper pressure and blood flow rates in the pulmonary arteries are of primary importance. Also, elevation of the post-operative central venous pressure should be avoided for an operation to be termed successful. Achieving these goals poses a challenge to surgical doctors who conduct TCPC surgical procedures.

In the past two decades, extensive efforts have been devoted to experimental exploration into the underlying blood flow transport mechanism in the vascular system. These investigations have made significant contributions to our understanding of vascular disease. Experimental success in conducting blood flow visualization has, however, been overshadowed by increasingly higher costs and the time-consuming nature of the process. Most serious is that it is still infeasible to use working fluids with the same characteristics as blood. In recent years, improvements in hardware and software have enabled investigators to use computational techniques to investigate complex hemodynamics in greater detail [6]. This article presents our recent research into the modeling of blood flow in the human vascular system.

2. Mathematical model

Numerical modeling of blood flow requires solving three-dimensional transient-flow equations in the time-varying physical domain. In this sense, the fluid and solid are allowed to move to follow the distensible vessels and deforming fluid subdomain. The need to conduct analysis in deformable blood vessels complicates the analysis. Use of a much more sophisticated numerical model, such as an arbitrary-Lagrangian–Eulerian (ALE) model [7, 8], is warranted in the vascular flow circulation analysis. According to surgical reports, the vessel diameter change per cardiac cycle is around 5–10% in most of the major arteries. As a first approximation, our assumption made here is that the vessel walls are regarded as being rigid.

To further simplify the analysis, the vessel is considered symmetric about the midplane (x–y plane) and this plane is taken as the domain of the solution as illustrated in Fig. 2. As a first attempt toward investigation into the hemodynamics in the human vascular system, we

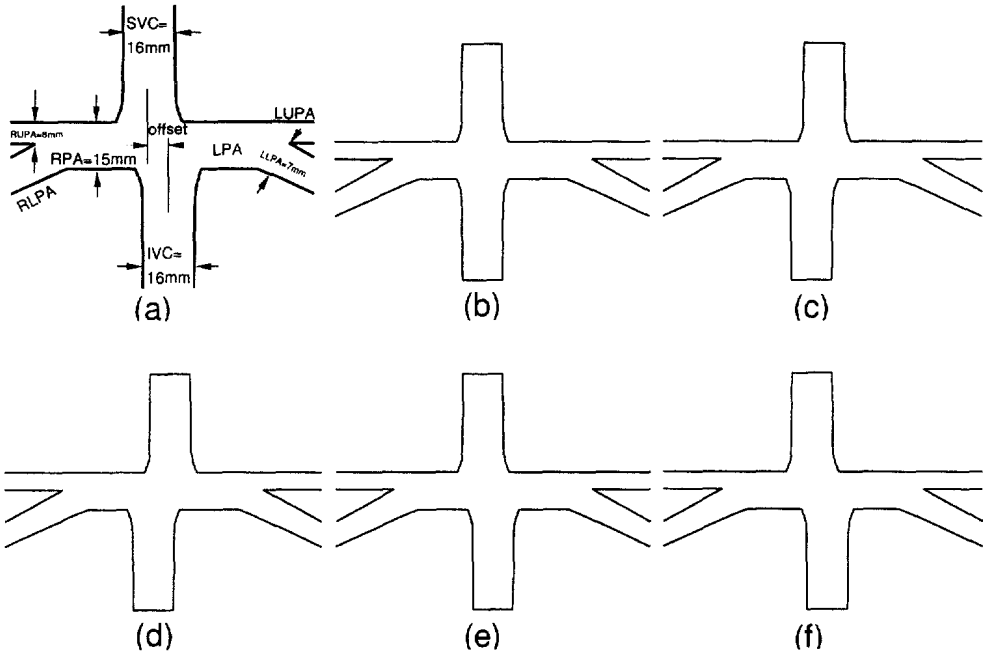

Fig. 2. Geometric configurations of the TCPC models: (a) schematic diagram of the TCPC model with bifurcation; (b) offset value = 0 mm; (c) offset value = 5 mm; (d) offset value = 7 mm; (e) offset value = −4 mm; (f) offset value = −6 mm.

performed laminar flow analyses, and k–ϵ two equation turbulence modelling is a subject of future investigation. Other main assumptions made in the mathematical model are as follows: the blood under investigation is a Newtonian fluid, which is treated as being homogeneous and incompressible. Under these circumstances, working equations, adequate for steady blood flow simulation in the vascular system, Ω, are made dimensionless as follows:

$$\underline{u} \cdot \nabla \underline{u} = -\nabla p + \frac{1}{Re} \nabla^2 \underline{u}, \tag{1}$$

$$\nabla \cdot \underline{u} = 0. \tag{2}$$

According to the chosen reference length, L, and characteristic velocity, U, given later in the results and discussion Section, the Reynolds number shown in Eq. (1) is $Re = UL/v$, where v is the kinematic viscosity of the Newtonian fluid flow.

The velocity-pressure formulation has proved to be effective in the simulation of incompressible fluid flows. The reason for use of the primitive-variable formulation is due mostly to its accommodation of the closure boundary condition [9]. Given that differential Eqs. (1) and (2) are classified as elliptic, specification of boundary conditions at the entire boundary of the domain is required to close the differential system. We divide the boundary of Ω, namely Γ, as the sum of Γ_d and Γ_n, subject to the constraint condition $\Gamma_d + \Gamma_n = \{0\}$. Along the boundary of Γ_d, we specify $\underline{u} = \underline{g}$ while along a boundary with an outward normal direction $\underline{n}$, we impose a boundary condition given by $-p\underline{n} + 1/Re \times \partial \underline{u}/\partial n = \underline{f}$ [10].

We now seek the steady-state solutions of the Navier–Stokes and continuity equations. Our explanation for the choice to consider a steady problem is that the inlet flows of SVC and IVC are non-pulsatile type, see also Ref. [5] for a more detailed explanation. The finite element method, as the theory stands, can be useful for problems involving complex geometries. In this study, solutions of the problem governed by Eqs. (1) and (2) were obtained by means of the method of weighted residuals. It is crucial that the velocity vector field accommodates the divergence-free property. To achieve this goal, we adopted the mixed formulation, see e.g. Ref. [13]. First, we denote by $\mathcal{L}^2(\Omega)$ the space of functions that are square integrable over Ω. We then define the constrained space $\mathcal{L}_0^2(\Omega) = \{q \in \mathcal{L}^2(\Omega) = \int_\Omega q \, d\Omega = 0\}$. This implies that $\mathcal{L}_0^2(\Omega)$ consists of square integrable functions having zero mean over Ω. In the mixing finite element formulation of Navier–Stokes equations we need to define the Sobolev space $\mathcal{H}^1(\Omega) = \{q \in \mathcal{L}^2(\Omega) : \mathcal{D}q \in \mathcal{L}^2(\Omega)\}$. Here, $\mathcal{D}$ denotes the derivative of order 1. Let the subspace of $\mathcal{H}^1(\Omega)$, namely $\mathcal{H}_0^1(\Omega)$, be the space whose elements have one square integrable derivative over Ω and vanish on the boundary Γ: $\mathcal{H}_0^1(\Omega) = \{q \in \mathcal{H}^1(\Omega) : q = 0 \text{ on } \Gamma\}$. With these functional space definitions, we can present the weighted residuals statement for the mixed finite element formulation as follows: given an admissive function $\underline{w} \in \mathcal{H}_0^1(\Omega) \times \mathcal{H}_0^1(\Omega) \equiv H_0^1$ and a pressure mode $q \in \mathcal{L}_0^2(\Omega) = \mathcal{P}$, find solutions of $(\underline{u}, p) \in V \equiv H_0^1 \times \mathcal{P}$ from the following equations:

$$\int_\Omega (\underline{u} \cdot \nabla \underline{u}) \cdot \underline{w} \, dx + \frac{1}{Re} \int_\Omega \nabla \underline{u} : \underline{w} \, d\underline{x} + \int_\Omega p \nabla \cdot \underline{w} \, d\underline{x} = \int_{\Gamma_n} \underline{w} \cdot \underline{f} \forall \underline{w} \in H_0^1, \tag{3}$$

$$\int_\Omega (\nabla \cdot \underline{u}) q \, d\underline{x} = 0 \quad \forall q \in \mathcal{P}. \tag{4}$$

More precisely, if Neumann conditions are adopted on outflow, $\underline{w} \notin H_0^1$, but $\underline{w} \in H_{\Gamma_d}^1$, where Γ_d is the Dirichlet boundary.

In mixed finite element analysis of incompressible fluid flows, choices of basis spaces for primitive variables are not arbitrary. Instead, the analysis is subjected to the inf–sup stability condition [11]. Violation of this condition will definitely result in spurious pressure modes and, in extreme cases, locking of the velocity field [12]. For this study, we approximate velocities in bi-quadratic elements and pressure in bi-linear elements, leading to a stable element-pair for incompressible flow simulations.

2.1. Streamline upwind Petrov–Galerkin model in quadratic elements

In finite element analysis of high Reynolds number flows, we need to define test function spaces that are appropriately applied to continuity and momentum equations. Given that the representative equation for the pressure takes a Poisson type through the use of a continuity equation, it is rational to use pressure basis functions as our test functions for the continuity equation given in Eq. (4). As advection terms become increasingly important, the upwind model is desirable. The motivation behind seeking the Petrov–Galerkin method as our upwind technique is due to the physical consideration. By doing so, test function $\underline{w}$ is chosen to be different from basis functions for u and v in the sense that more weights are logically placed on

the upstream side of the preferred flow direction. In this way, numerical oscillations and instabilities can be prevented in the high Reynolds number case. The method adopted here is considered to be in the Petrov–Galerkin framework [13].

Upwind models, while acceptable for stability enhancement, may not be adequate to approximate advection terms in a domain with more than one spatial dimension. The accuracy of the prediction may deteriorate due to the introduction of so-called false diffusion errors [14]. As our ultimate intention was to obtain flow details, we needed to improve further the accuracy of the multi-dimensional flow prediction. The philosophy underpinning this effort was to avoid crosswind diffusion but not at the expense of compromising stability. To achieve this goal, test functions w_i were constructed by adding unequally weighted functions B_i, which were cast in a tensorial-product form as follows, to trial function N_i

$$B_i = \tau N^j \tilde{V}_k^j \frac{\partial N^i}{\partial x_k} \tag{5}$$

where

$$\tau = \frac{\delta(\gamma)}{2 \mid \underline{u} \mid^2}. \tag{6}$$

In the above equation, $\tilde{V}_k$ stand for velocities which are evaluated at element centroids. The coefficient δ, which is written as a function of the Peclet number, $\gamma = \mid \underline{u} \mid h/2\mu$, remained to be determined. In this study, the coefficient δ, which determines the degree of upwinding, is analytically derived from the one-dimensional convection–diffusion scalar transport equation in quadratic elements. Readers are referred to Ref. [15] for additional details. Depending on the nodal classification in quadratic elements, analytic expressions have been obtained as follows:

$$\delta(\gamma) = \begin{cases} \frac{1}{2}\coth\left(\frac{\gamma}{2}\right) - \frac{1}{\gamma} & \text{; center-nodes,} \\ \dfrac{\gamma \sinh\gamma \cosh\gamma - \sinh^2\gamma - 4\cosh\gamma - 2\gamma\sinh\gamma - 4}{6\sinh\gamma\cosh\gamma + \gamma\sinh^2\gamma - 6\sinh\gamma - 4\gamma\cosh\gamma + 4\gamma} & \text{; corner-nodes.} \end{cases} \tag{7}$$

Before entering into a discussion of the results, it is worthwhile to address some fundamental features of the proposed upwind model. Firstly, biased weighting functions were applied to each term shown in the momentum equations. This led to the satisfaction of the scheme consistency property. Secondly, since a fundamental understanding of how discretization schemes affect the prediction accuracy, it is useful to conduct a modified equation analysis for the transport of a scalar variable Φ. The equation under investigation resembles the linearized momentum equation given as follows:

$$a\Phi_x + b\Phi_y = -p_x + k(\Phi_{xx} + \Phi_{yy}). \tag{8}$$

As the following modified equation shows, application of the Petrov–Galerkin method to Eq. (8) introduces a stabilizing term which is added solely to the flow direction.

$$a\Phi_x + b\Phi_y + p_x - k(\Phi_{xx} + \Phi_{yy}) = (a^2 + b^2)\tau\Phi_{ss} + O(h^2). \tag{9}$$

Lastly, the derivation of δ is only analytically feasible on a one-dimensional basis.

3. Problem description

A problem of considerable clinical importance in Fontan procedures concerns blood flow distribution in the TCPC (total cavopulmonary connection). According to the anatomy of the TCPC, which is shown in Fig. 3, blood flows from the SVC (superior vena cava) and IVC (inferior vena cava) are confluent at the *T*-junction. This is followed by a downstream flow into the left pulmonary artery (LPA) and right pulmonary artery (RPA). Downstream from the confluence of the SVC and IVC, the main pulmonary artery bifurcates into four branches, namely, the left upper pulmonary artery (LUPA), left lower pulmonary artery (LLPA), right upper pulmonary artery (RUPA), and right lower pulmonary artery (RLPA). These branch flows proceed further downstream to the left and right lungs shown schematically in Fig. 1(b).

This study was based on a clinical case treated at the National Taiwan University Hospital. According to measurements from angiocardiograms, the vessel diameters under investigation were 16 mm for the SVC and the IVC, 7 mm for the LUPA and RUPA, and 8 mm for the RLPA and LLPA, respectively. The diameter of both the RPA and LPA was 15 mm. For better flow distribution and energy dissipation, surgical reasoning suggests the enlargement of the IVC and SVC anastomoses. As the main pulmonary was approached, the diameter of the SVC and IVC increased gradually, reaching 130% diameter enlargement at the IVC and SVC anastomoses.

As clinical reports indicate, the SVC, carrying approximately one third of the systemic venous return, goes preferentially to the larger right lung. As a result, the IVC flow carries two-thirds of the systemic venous return and goes to the smaller left lung. Recognizing this, it is a considerable incentive to prescribe a Dirichlet type boundary condition at inlets of the IVC and SVC. For ease of simulation, the flow conditions at the inlets of the SVC and IVC were all non-pulsatile types with a steady parabolic velocity profile. The flow rates at the inlets of the

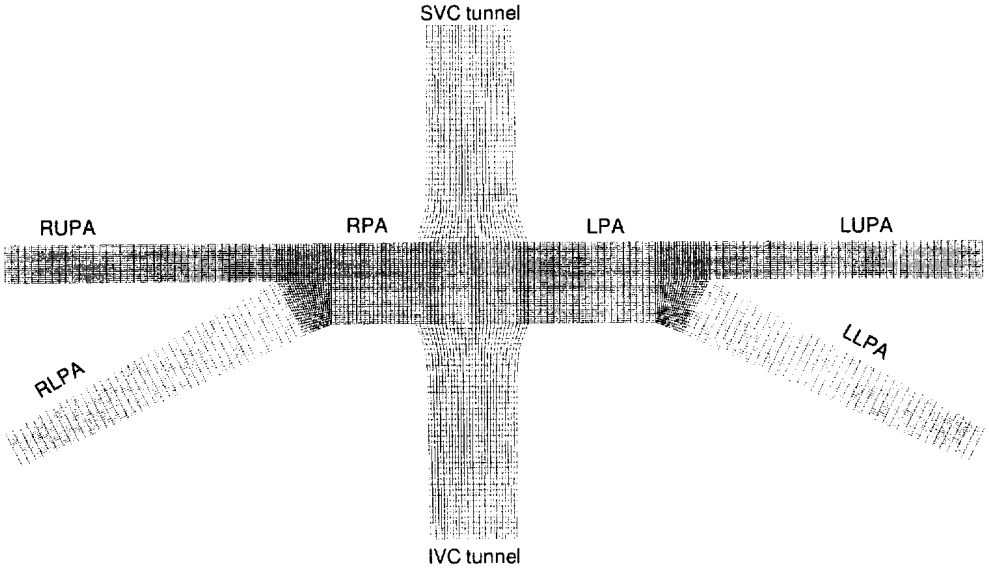

Fig. 3. Computational mesh for the TCPC model.

SVC and IVC were kept constant throughout simulations considered here. According to the diameters of the vessels and the volume flow rates, namely $Q_{IVC}=2$ l/min and $Q_{SVC}=1$ l/min, the maximum inlet velocities of the IVC and SVC were obtained as 0.256 m/s and 0.128 m/s, respectively. According to the density, $\rho = 1060$ kg/m^3, and viscosity of the Newtonian blood, $\mu = 3 \times 10^{-3}$ Pa s, the Reynolds number under investigation was 565. This number was the result of regarding $D = 0.016$ m as the reference length and $U=0.1$ m/s as the characteristic velocity. To close the target elliptic-type differential system, there remained the specification of boundary conditions at the outlet. In the numerical simulation of inflow–outflow problems featuring the incompressible fluid flows, appropriate specification of inflow–outflow boundary conditions is challenging. In Ref. [16], suitable inflow and outflow boundary conditions are considered. Due to the presence of the lungs, through which LUPA, LLPA, RUPA, and RLPA circulate, there is a tendency to impose a resistance force to the flowing blood moving towards the lungs. This further complicates the analysis. According to the work of de Leval et al. [17] who prescribed constant pressure at the outlet sections, analysis of TCPC blood flow was conducted by coupling Navier–Stokes flow calculations with the lumped-parameter model of the pulmonary circulation. The other assumptions made in their mechanical model of pulmonary circulation were that both elastic compliances and inertia effects were absent, leading to a sole resistance component. Due to the lack of pulmonary resistance and left atrium pressure, which are usually included in the cardiac catheterization report, an alternative approach was adopted to close the differential system. For this study, the free boundary condition approach [10] was applied at four outlet sections. The free boundary condition approach is featured by regarding $\underline{f}$, given in Eq. (3), as unknown in the sense that $\underline{f} = -p\underline{n} + 1/Re \times \partial \underline{u}/\partial n$. As a result, $\underline{f}$ serves as a part of the solutions to be computed. This approach differs from the work of Leval et al. [17] who assumed constant pressure values prescribed at the truncated outlets. For clearness, we summarize our discretized equations formulated in biquadratic velocity-bilinear pressure elements as follows:

$$\left[\int_{\Omega^h}\begin{Bmatrix} C^{ij} & 0 & -M^j\frac{\partial N^i}{\partial X^1}+B_i\frac{\partial M^j}{\partial X_1} \\ 0 & C^{ij} & -M^j\frac{\partial N^i}{\partial X_2}+B_i\frac{\partial M^j}{\partial X_2} \\ M^i\frac{\partial N^i}{\partial X_1} & M^i\frac{\partial N^j}{\partial X_2} & 0 \end{Bmatrix} d\Omega^h\right]\begin{pmatrix} u_j \\ v_j \\ p_j \end{pmatrix} = \int^h{}_{\Gamma_{outlet}} N^i \begin{pmatrix} -pn_x+\frac{1}{Re}\frac{\partial u_j}{\partial n} \\ -pn_y+\frac{1}{Re}\frac{\partial v_j}{\partial n} \\ 0 \end{pmatrix} d\Gamma^h \tag{10}$$

In Eq. (10), M^i are biquadratic polynomials and N^i are bilinear polynomials.

Numerous factors may have appreciable impact on the hydrodynamic characteristics. For example, the movement of the IVC anastomosis alongside the pulmonary artery helps improve the balance between flow distribution and energy dissipation [17]. In this study the attention is only given to studying the effect of the offset on two important energy indexes, namely, the hydraulic dissipated power, W_d, and the total energy-loss coefficient C_e. These definitions will be given later in the results and discussion Section. Throughout this study, the axes of symmetry of both the IVC and SVC are kept normal to the pulmonary artery. For this study, results are shown only as functions of the offset, which is defined as the distance between the centers of two caval anastomoses. Following the definition employed in Ref. [17], the negative offset is that the anastomoses of the IVC is displaced toward the reader's right side. For five

offsets under investigation (Fig. 2), our goal was to optimize the flow after TCPC surgical intervening such that energy-loss is reduced and flow distribution between the two lungs is optimized.

4. Results and discussion

Computations were conducted under laminar assumption for five configurations, as shown in Fig. 2. These configurations differ simply in their offset values. Grid sensitivity tests revealed that 2500 elements were adequate to resolve the flow recirculation over the Reynolds number considered in this work. Fig. 3 gives an overview of the mesh of quadratic finite elements. The grids were packed near the vessel wall where the boundary layer profile may develop. Grids were also clustered in regions where the vessel may undergo a marked change in its configuration to better resolve flow separation or recirculation in the flow. The geometrical complexity creates additional complexities to model nonlinearities in the equations, tending to make it difficult for the analysis to converge. It is, thus, important to assure that the results are indeed the convergent solutions. In this regard, we plotted in Fig. 4 the convergence histories for all the primitive variables against iterations. For this study, $u^{k+1}-u^k$, $v^{k+1}-v^k$, and $p^{k+1}-p^k$ were all cast in their L_2-norm forms, where superscripts k and $k+1$ denoted two consecutive iteration numbers. The convergence histories presented in Fig. 4 serve to demonstrate the applicability of the proposed finite element code to model the hemodynamics in vascular circulation.

With the computed convergent solutions, we can next explore the physics in the blood flow. Our aim was to gain some useful insights from the prediction results. To give readers a global

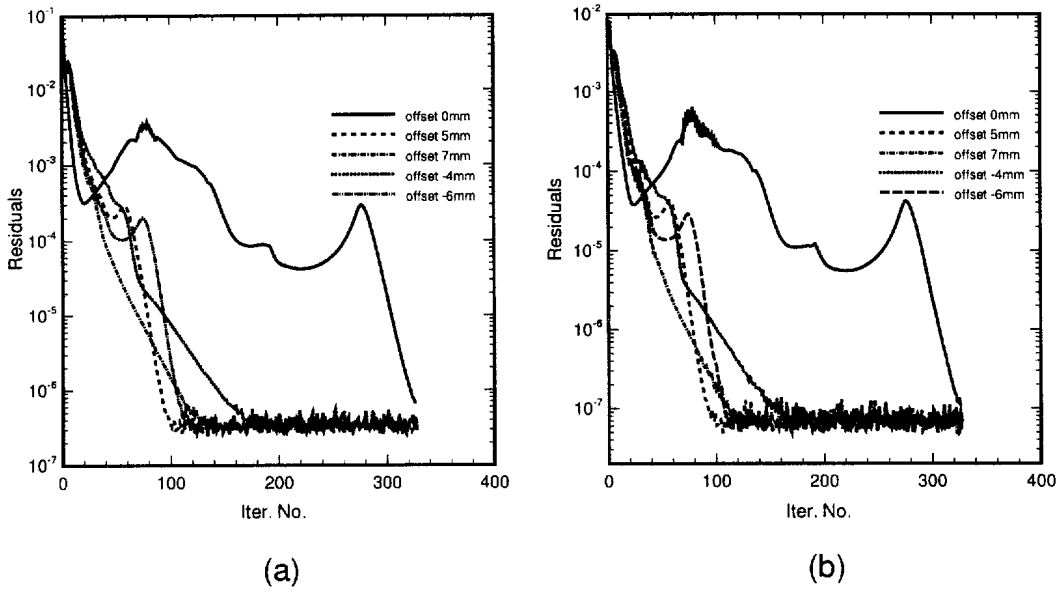

Fig. 4. Residual reduction histories for five investigated TCPC configurations: (a) velocities; (b) pressure.

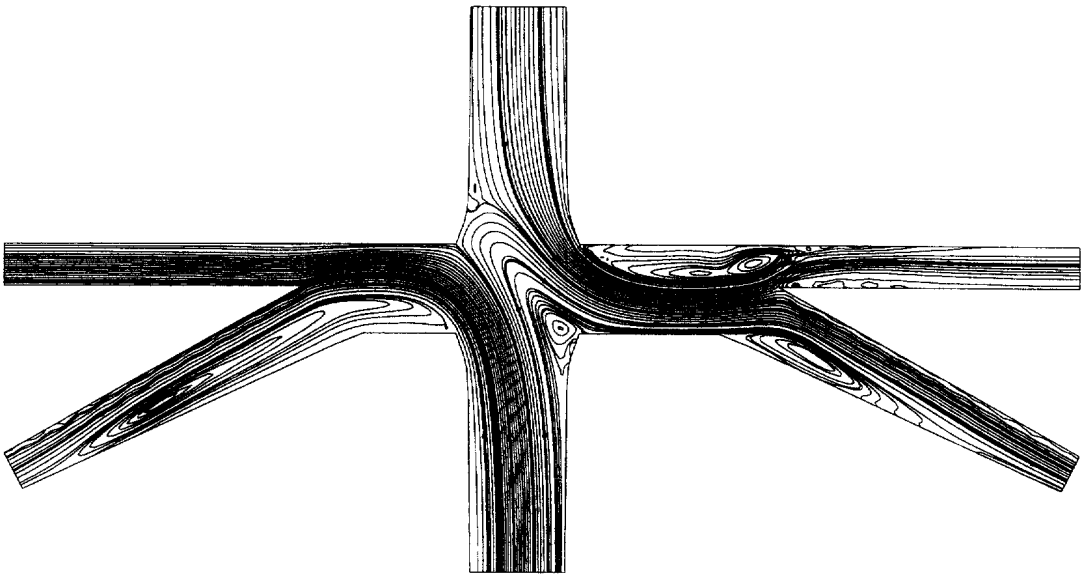

Fig. 5. Predicted streamline contours for the case with the offset of 0 mm.

picture of the flow structure in the blood vessel with bifurcations, we plotted in Figs. 5–9 the computed streamline contours for five offset values. Common to these figures is the presence of flow reversals. For offset values other than zero, the sizes of the recirculation regions in the confluence area of the IVC and SVC as well as the intensity of the vorticities increase. In the T-junction, the bloods in the SVC and IVC are with flow directions which are opposite to each

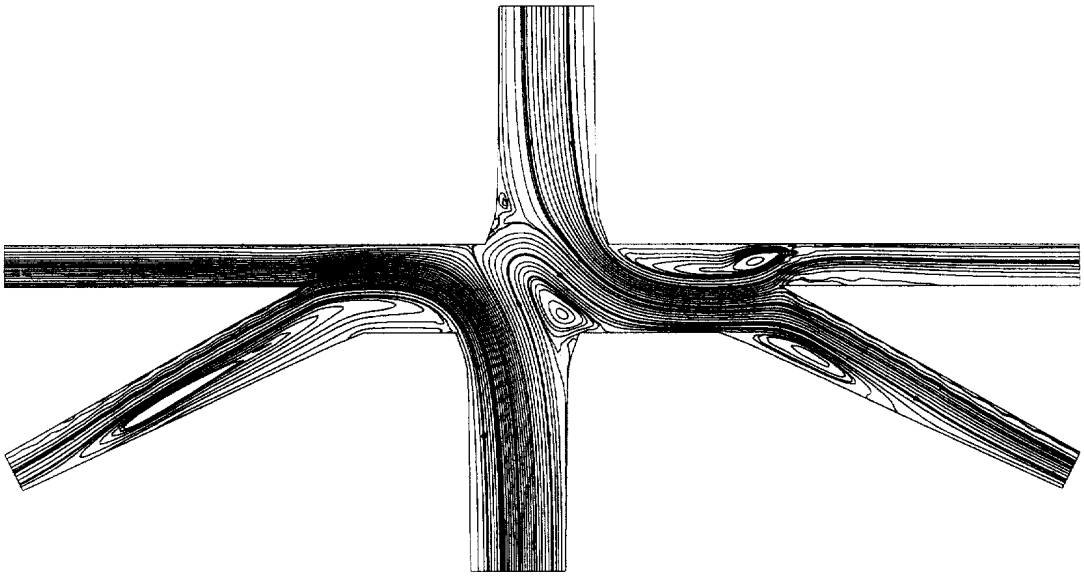

Fig. 6. Predicted streamline contours for the case with the offset value of 5 mm.

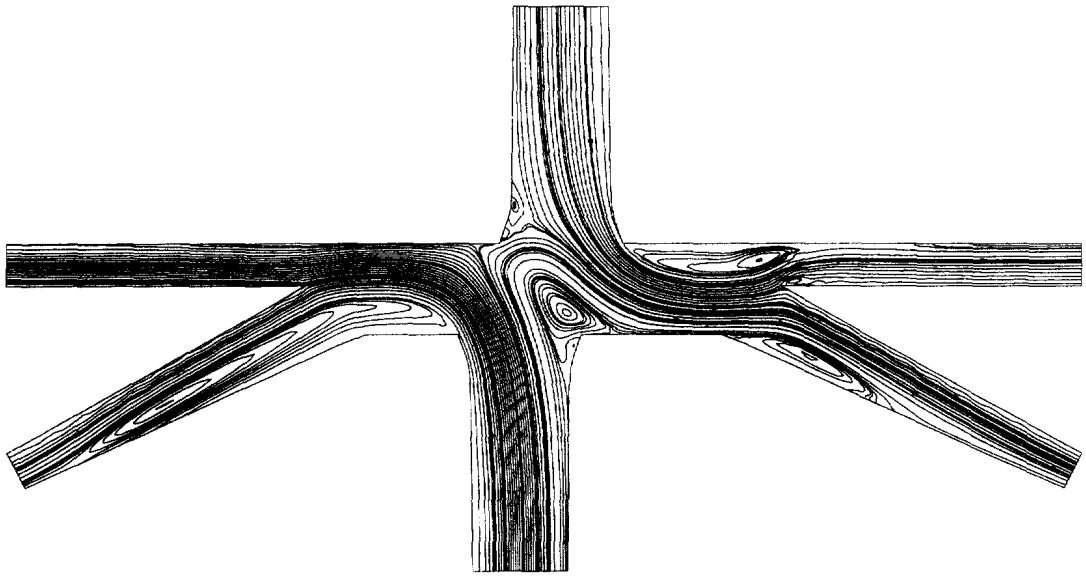

Fig. 7. Predicted streamline contours for the case with the offset value of 7 mm.

other. In the presence of such opposite flow directions in the pulmonary artery, together with abrupt changes in geometry and velocity, the energy loss inevitably resulted. We will discuss this issue later.

For the sake of description of the flow pattern, we take the case with the offset value—4 mm (Fig. 8) for an example in this paragraph. As compared with the LPA, the pulmonary artery

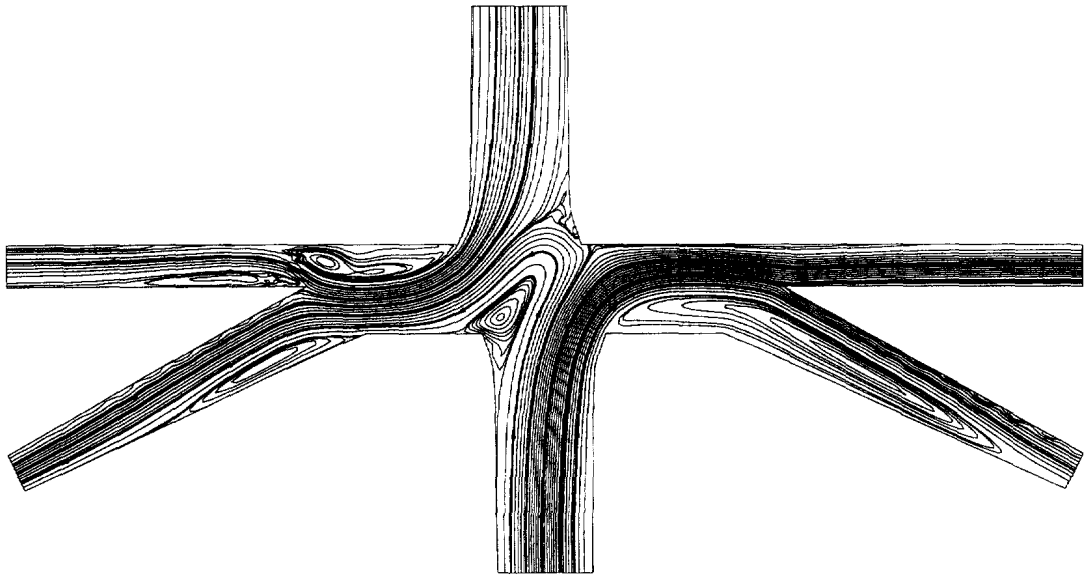

Fig. 8. Predicted streamline contours for the case with the offset value of –4 mm.

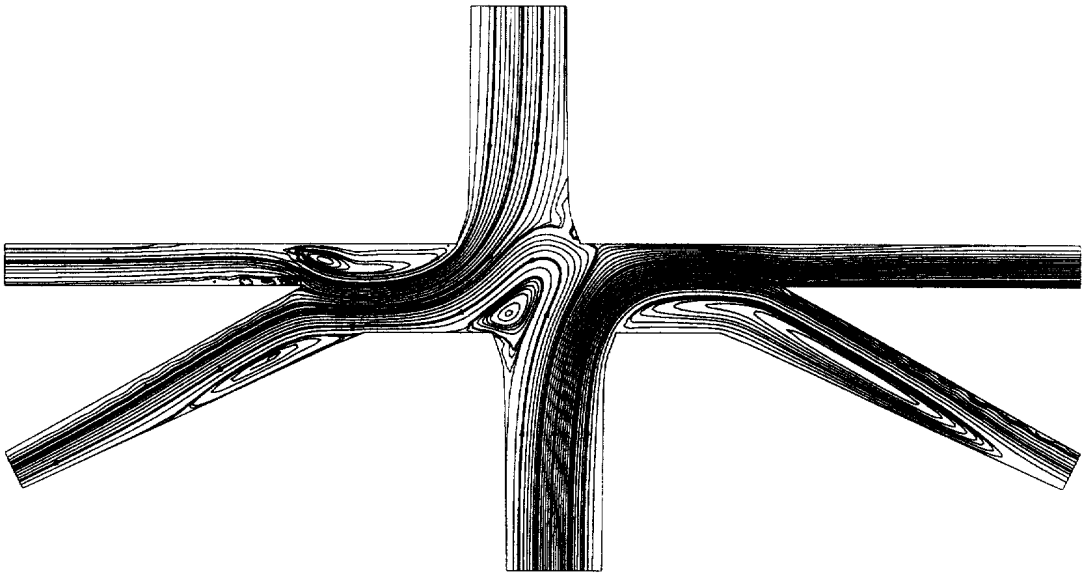

Fig. 9. Predicted streamline contours for the case with the offset value of −6 mm.

extends further downstream before the RPA bifurcates into the RUPA and RLPA. It is this difference which causes the SVC blood to flow mainly towards the RPA while blood in the IVC flows towards the LPA. Such a flow distribution pattern explained, in turn, why a circulation bubble has been observed only in the upper RPA. The location where the recirculation bubble forms was upstream of the bifurcation point. The mechanism leading to the formation of flow reversal is the resistance of the pressure force established near the bifurcation point, which served as a singular point. On each lower branch of the pulmonary arteries, flow reversals were observed. They differed in their size of flow reversals. The reason for the formation of two recirculation regions is mainly due to the flow expansion. Compared to the expansion eddy in the right pulmonary artery, the left pulmonary artery is much larger. This accounted for the appreciable flow curvature observed in the curved flow due to the presence of the upper flow reversal in the right pulmonary artery. Another explanation for the marked expansion eddy observed in the left pulmonary artery is the shorter length which allows the flow development into the left branch of the vessel.

As Figs. 5–7 show, curved flows are a consequence of the *T*-junction flow. As noted earlier, blood in the SVC flows mostly to the RPA, resulting in the left SVC vessel being the pressure side while the inner wall is the suction side (Fig. 10). On the other hand, the pressure side of the IVC vessel is on the reader's left side while the suction side of the IVC vessel is regarded as the suction side. This explains why flow reversals in the confluence regime are observed on the pressure side. To provide readers insight into the flow development into the pulmonary artery, we plotted in the vessel the velocity profiles at some selected sections. As Fig. 11–16 show, one can clearly see why the local velocity maximums in the IVC and SVC were observed along the suction side. Flow reversals were also clearly seen from the streamline contour plots, shown in Figs. 5–9.

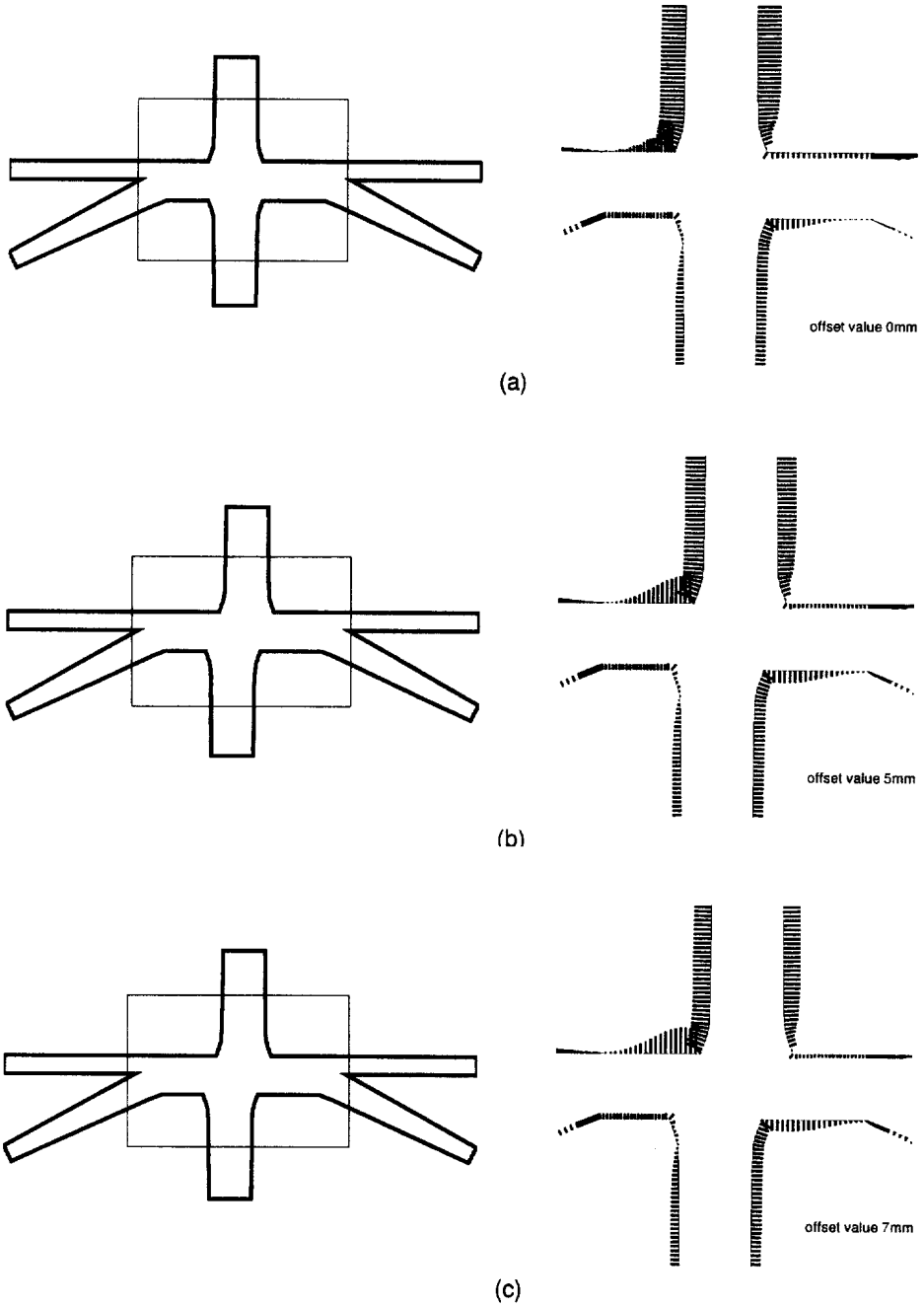

Fig. 10. Pressure applied on the vessel walls: (a) offset value = 0 mm; (b) offset value = 5 mm; (c) offset value = 7 mm.

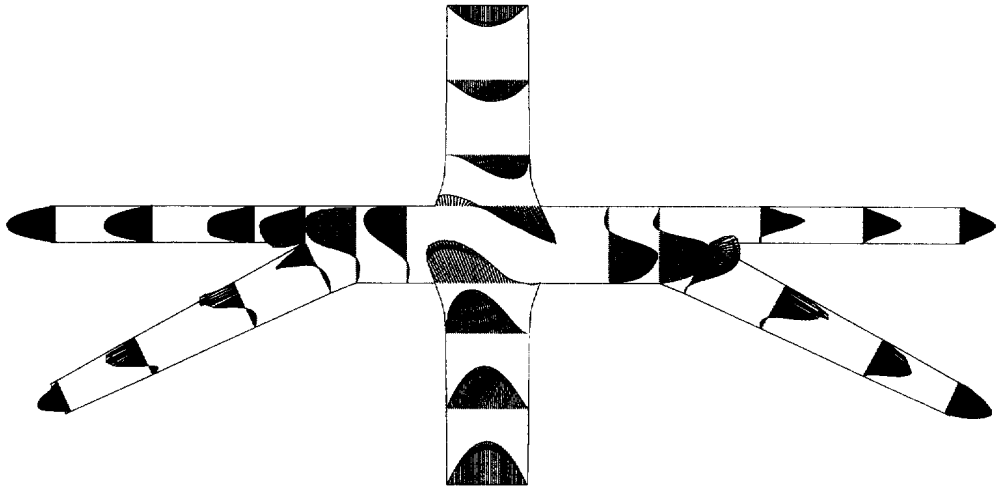

Fig. 11. Computed midplane velocity vectors at selected sections in the TCPC model with the offset value of 0 mm.

In an attempt to explore in greater detail the recirculating flow structure in the T-junction with geometrical bifurcations, we depicted the flow topology based on the topology theory of Legendre [18]. Based on the computed velocities, we can determine critical points in the blood vessel. According to the topological classification, critical points can be termed as separation, reattachment, spiral, and saddle points. We marked in Figs. 16–20 the point of separation with an '•', the point of reattachment with an '○', the point of spiral with an '*', and the saddle point with an ' × '. Revealed by Figs. 16–20 are saddle points in the confluence region of the IVC and SVC. Within the recirculatory bubbles, spiral points are captured. This is an indication of the emergence of the core of the vortical flow.

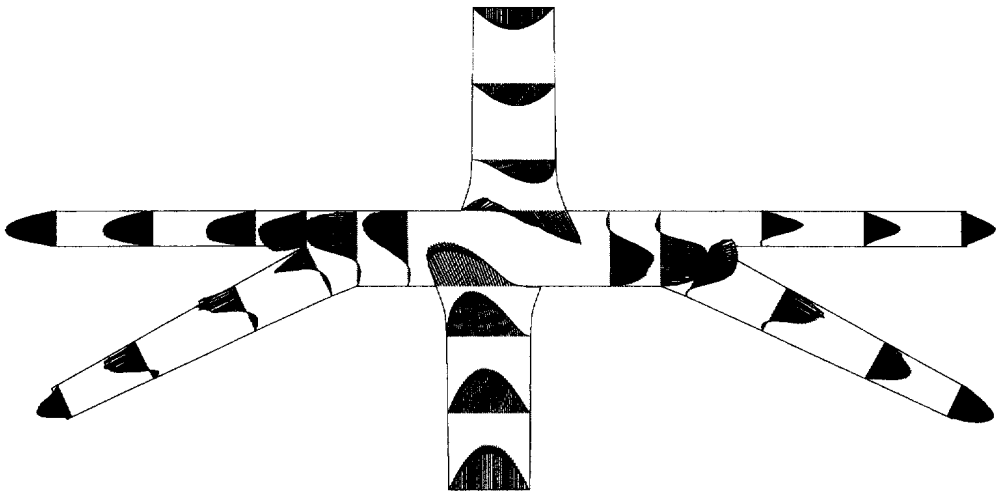

Fig. 12. Computed midplane velocity vectors at selected sections in the TCPC model with the offset value of 5 mm.

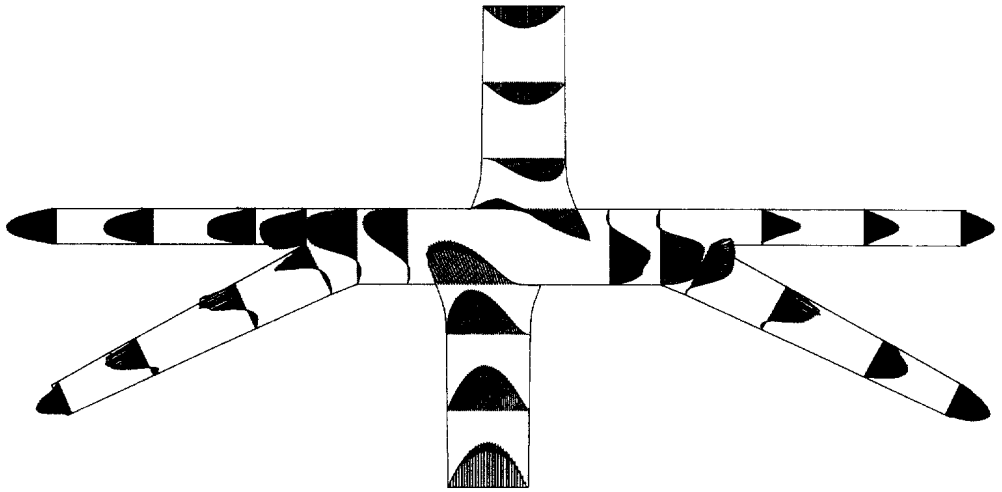

Fig. 13. Computed midplane velocity vectors at selected sections in the TCPC model with the offset value of 7 mm.

As clinical reports show, the best flow distribution between the right and left lung is considered to be 55% to the right lung and 45% to the left. The distribution of blood is, thus, a crucial factor in TCPC operations. This has motivated us to study blood distribution for operations performed at different offset values. To accomplish this task, we have integrated the computed velocities at four outlet planes to render the volumetric flow. We showed them in Table 1 for five investigated offsets. As noted earlier in the numerical prediction of the *T*-junction, the marked change in configuration inevitably resulted in an energy loss. Better design of connections in TCPC surgical operations involves consideration of energetic indices. Two important parameters are often referred to. The first one is the total energy loss coefficient

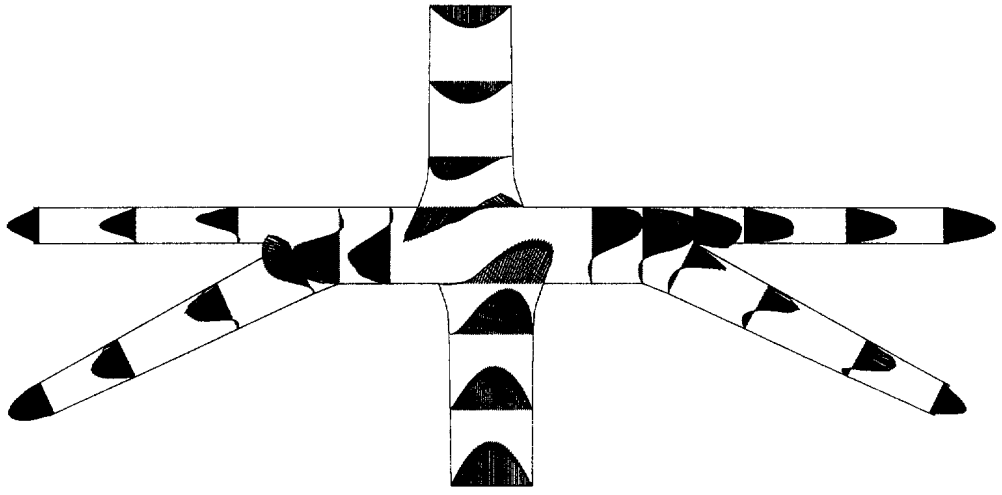

Fig. 14. Computed midplane velocity vectors at selected sections in the TCPC model with the offset value of −4 mm.

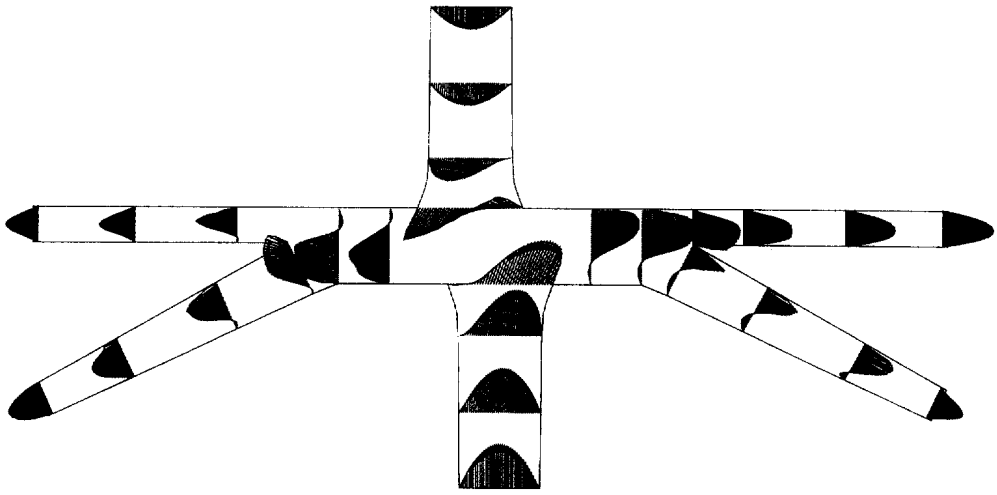

Fig. 15. Computed midplane velocity vectors at selected sections in the TCPC model with the offset value of −6 mm.

C_e, defined as follows:

$$C_e = \frac{(\frac{1}{2}\rho V_{\mathrm{IVC}}^2 + P_{\mathrm{IVC}})Q_{\mathrm{IVC}} + (\frac{1}{2}\rho V_{\mathrm{SVC}}^2 + P_{\mathrm{SVC}})Q_{\mathrm{SVC}} - \Sigma_i(\frac{1}{2}\rho V_i^2 + P_i)Q_i}{\frac{1}{2}\rho(V_{\mathrm{IVC}}^2 Q_{\mathrm{IVC}} + V_{\mathrm{SVC}}^2 Q_{\mathrm{SVC}})},$$

$$i = \mathrm{LUPA, LLPA, RUPA, RLPA.} \tag{11}$$

The other indicator of prime importance is the hydraulic power given below:

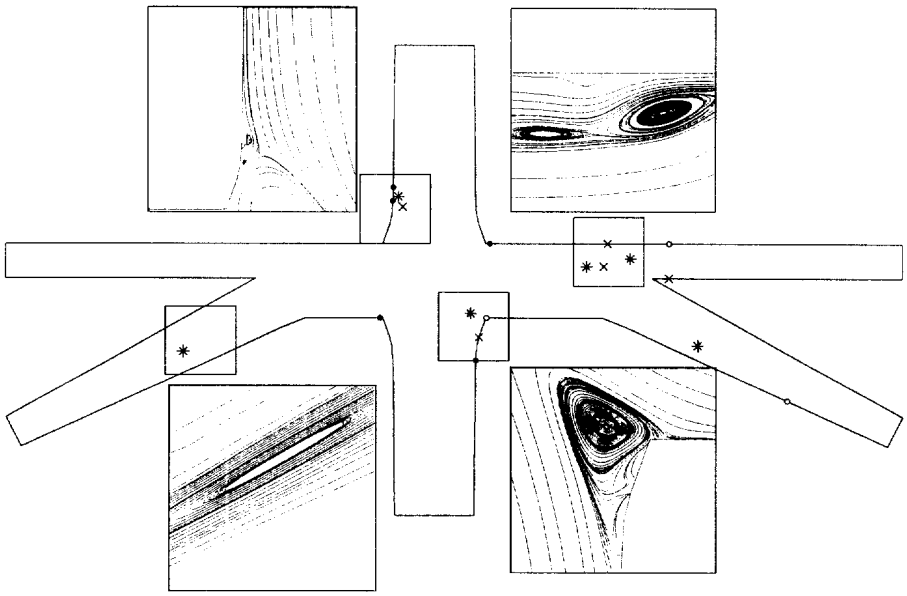

Fig. 16. Flow details in regions with critical points for the case with the offset value of 0 mm. [separation point (●); reattachment point (○); spiral point (*); saddle point (×)].

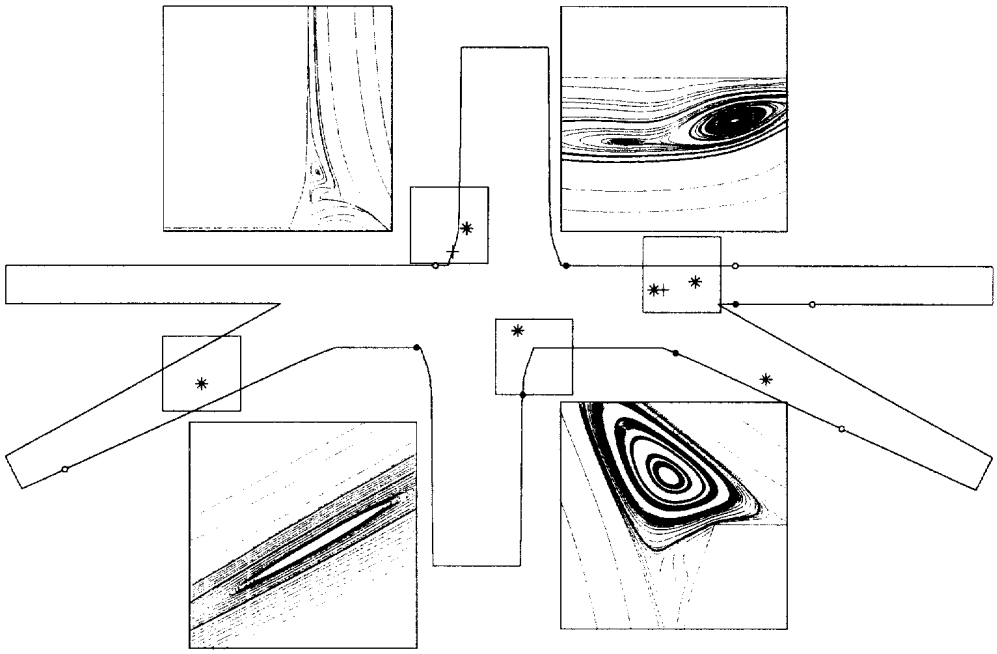

Fig. 17. Flow details in regions with critical points for the case with the offset value of 5 mm. [separation point (•); reattachment point (○); spiral point (*); saddle point (×)].

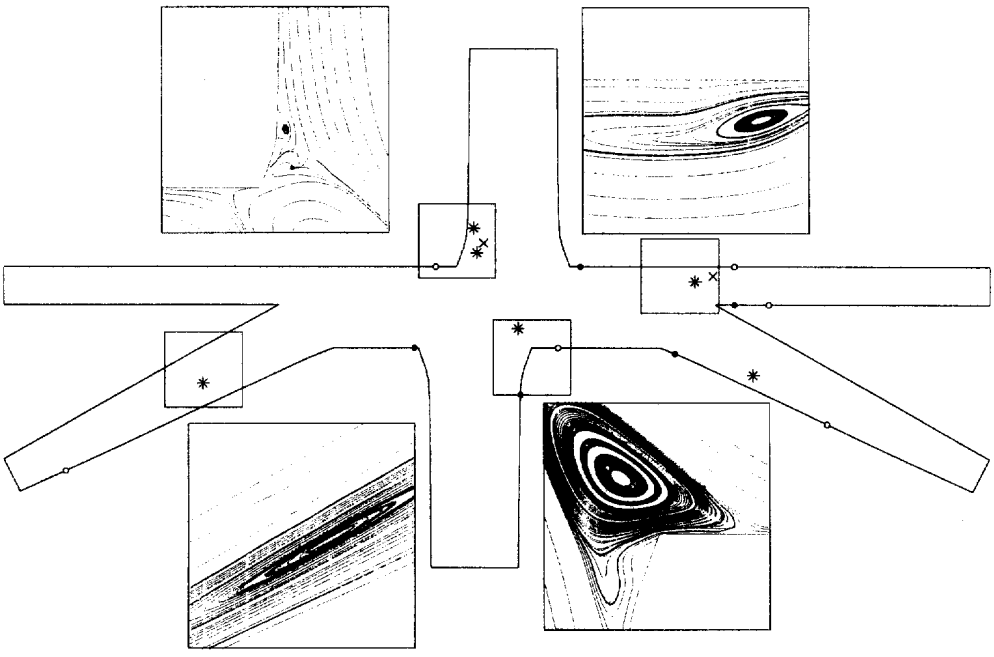

Fig. 18. Flow details in regions with critical points for the case with the offset value of 7 mm. [separation point (•); reattachment point (○); spiral point (*); saddle point (×)].

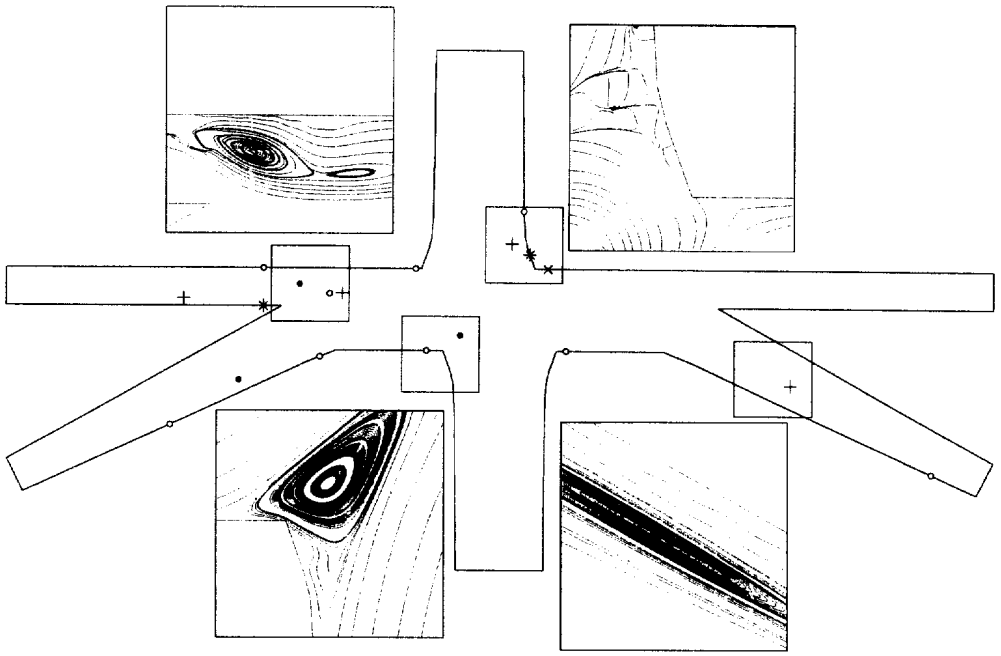

Fig. 19. Flow details in regions with critical points for the case with the offset value of −4 mm. [separation point (•); reattachment point (○); spiral point (*); saddle point (×)].

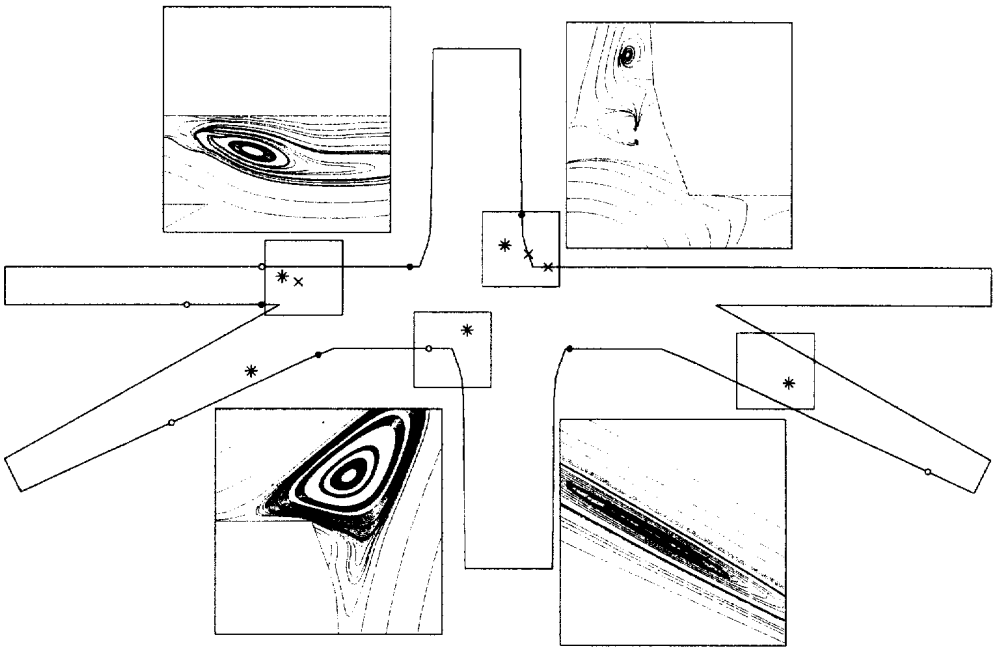

Fig. 20. Flow details in regions with critical points for the case with the offset value of −6 mm. [separation point (•); reattachment point (○); spiral point (*); saddle point (×)].

Table 1
Results of quantities that are needed in the determination of C_e and W_d in Eqs. (11) and (12) for the TCPC simulations

	Q	$\bar{V}$	$\bar{P}$	$(\frac{1}{2}\rho\bar{V}^2)Q$	Total	$(\frac{1}{2}\rho\bar{V}^2+\bar{P})Q$	Total
	Offset 0 mm						
IVC	0.002726	0.1704	13.0287	0.0649		2.8262	
SVC	0.001363	0.0852	34.1448	0.0081	0.073	1.4176	4.2438
RUPA	0.001394	0.2006	−0.5118	0.0436		1.4365	
RLPA	0.000664	0.1069	0.0064	0.0061		0.6705	
LUPA	0.000843	0.1284	−0.0521	0.0117		0.8542	4.1619
LLPA	0.001175	0.1790	−1.9861	0.0283		1.2007	
	Offset 5 mm						
IVC	0.002726	0.1704	13.7936	0.0649		2.8283	
SVC	0.001363	0.0852	27.7241	0.0081	0.073	1.4088	4.2371
RUPA	0.001407	0.2021	−0.5792	0.0449		1.4507	
RLPA	0.000771	0.1078	0.0187	0.0074		0.7188	
LUPA	0.000801	0.1158	−0.0519	0.0098		0.8105	4.1610
LLPA	0.001157	0.1751	−1.6794	0.0259		1.1810	
	Offset 7 mm						
IVC	0.002726	0.1704	13.2244	0.0649		2.8268	
SVC	0.001363	0.0852	24.8206	0.0081	0.073	1.4049	4.2317
RUPA	0.001397	0.2019	−0.4860	0.0439		1.4401	
RLPA	0.000726	0.1095	0.0381	0.0081		0.7337	
LUPA	0.000829	0.1201	0.0033	0.0104		0.8390	4.1564
LLPA	0.001122	0.1704	−1.4823	0.0234		1.1436	
	Offset −4 mm						
IVC	0.002726	0.1704	13.0287	0.0649		2.8306	
SVC	0.001363	0.0852	34.1448	0.0081	0.073	1.4107	4.2413
RUPA	0.000738	0.1065	−0.0988	0.0080		0.7455	
RLPA	0.001194	0.1807	−1.4660	0.0276		1.2202	
LUPA	0.001402	0.2027	−0.9208	0.0453		1.4463	4.1585
LLPA	0.000738	0.1122	0.0365	0.0082		0.7465	
	Offset −6 mm						
IVC	0.002726	0.1704	13.7388	0.0649		2.8282	
SVC	0.001363	0.0852	26.0674	0.0081	0.073	1.4066	4.2348
RUPA	0.000797	0.1145	−0.0247	0.0096		0.8066	
RLPA	0.001141	0.1726	−1.2762	0.0240		1.1636	
LUPA	0.001400	0.2021	−0.7022	0.0445		1.4431	4.1570
LLPA	0.000736	0.1111	0.0429	0.0081		0.7437	

$$\dot{W}_d = \left(\frac{1}{2}\rho V_{IVC}^2 + P_{IVC}\right)Q_{IVC} + \left(\frac{1}{2}\rho V_{SVC}^2 + P_{SVC}\right)Q_{SVC} - \sum_i \left(\frac{1}{2}\rho V_i^2 + P_i\right)Q_i,$$

$$i = \text{LUPA, LLPA, RUPA, RLPA.} \tag{12}$$

The computed C_e and W_d were shown in Table 2 and plotted in Fig. 21 for all five investigated offsets.

Table 2
Summary of results for W_{diss}, C_e and ratio of flow rates for five TCPC configurations

	W_{diss}	W_{diss}/W_{in}	C_e	Q_{RPA}/Q_{LPA}
Offset 0 mm	0.0819	1.9%	1.122	1.02
Offset 5 mm	0.0761	1.8%	1.142	1.082
Offset 7 mm	0.0753	1.78%	1.032	1.088
Offset −4 mm	0.0828	1.95%	1.134	0.903
Offset −6 mm	0.0778	1.84%	1.066	0.907

5. Conclusions

This paper describes numerical simulation of blood flow to the lung after a surgical procedure (TCPC Fontan procedure). Our strategy to simulate the flow in the neighborhood of a junction is to solve the full nonlinear steady Navier–Stokes equations using a streamline upwind finite element method. Through this study, we could draw a clear picture of the flow structure which helps us to better understand the effect of offset values on the blood distribution in the left and right pulmonary arteries. The role of the offset as a control parameter in the Fontan practice to optimize anastomoses between superior venae cavae and inferior venae cavae was examined in terms of the total energy-loss coefficient and the hydraulic dissipated power. Clearly revealed from this study is that for operations with a positive offset value they are the candidate for the TCPC surgical practice in the sense that more blood can flow towards the larger right lung. Of two investigated positive offset values, the one with 7 mm is our preference in that less energy loss is observed.

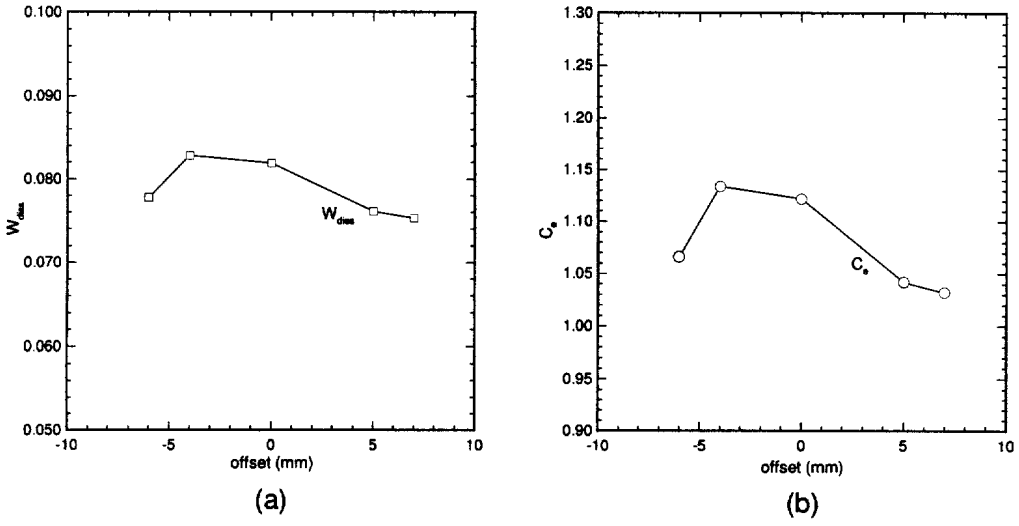

Fig. 21. (a) Hydraulic dissipated power W_{diss}, as difined in Eq. (12) vs offset values; (b) total energy loss, as defined in Eq. (11) vs offset values.

Acknowledgements

The authors would like to thank Prof I S Chiu, the Medical doctor and the congenital cardiac surgeon of National Taiwan University Hospital, who has provided useful knowledge in the course of conducting this medical study. Research support by the National Science Council under grant NSC 87-2213-E-002-002 is also gratefully acknowledged.

References

[1] Kim YH, Walker PG, Fontaine AA, Panchal S, Ensley AE, Oshinski J, Sharma S, Ha B, Lucas CL, Yoganathan AP. Hemodynamics of the Fontan connection: an in-vitro study. ASME J of Biomech Engng 1995;117:423.
[2] Fontan F, Baudet E. Surgical repair of tricuspid atresia. Thorax 1971;26:240,.
[3] Fontan F, Kirklin JW, Fernandez G, Costa F, Naftel DC, Tritto F, Blackstone EH. Outcome after a perfect Fontan operation. Circulation 1990;81:1520.
[4] de Leval MR, Kilner P, Gewiling M, Bull C. Total cavopulmonary connection: a logical alternative to atripulmonary connection for complex Fontan operation. J Thorac Cardiovasc Surg 1988;96(5):682.
[5] Dubini G, de Leval MR, Pietrabissa R, Montevecchi FM, Fumero R. A numerical fluid mechanical study of repaired congenital heart defects application to the total cavopulmonary connection. J Biomech 1996;29(1):111.
[6] Taylor C, Hughes T, Zarins C. Computational investigations in vascular disease. Comput Phys 1996;10(3):224.
[7] Hirt CW, Amsden AA, Cook JC. An arbitrary Lagrangian–Eulerian computing method for all flow speeds. J Comp Phys 1974;14:227.
[8] Hughes TJR, Liu WK, Zimmermann TK. Lagrangian–Eulerian finite element formulation for incompressible viscous flows. Comput Meth Appl Mech Engng 1981;29:329.
[9] Quartapelle L. Numerical solution of the incompressible Navier–Stokes equations. Berlin: Birkhäuser, 1993.
[10] Wang MT, Sheu TWH. Implementation of a free boundary condition to Navier–Stokes equations. Int J Numer Meth H&F Fl 1997;7(1):95.
[11] Brezzi F. On the existence, uniqueness and approximation of saddle point problems arising from Lagrangian multipliers. RAIRO, Anal Num 1974;129:.
[12] Babuška I. Error bounds for finite element methods. Numer Math 1971;16:322.
[13] Quarteroni A, Valli A. Numerical approximation of partial differential equations. Berlin: Springer, 1994.
[14] Leonard BP. A stable and accurate convective modelling procedure based on quadratic upstream interpolation. Comput Meth Appl Mech Engng 1979;19:59.
[15] Sheu TWH, Tsai SF, Wang MMT. Discussion of numerical deficiency of applying a partially-weighted upwind finite element model to incompressible Navier–Stokes equations. Num Ht Trans part B: fundamentals 1997;32:197.
[16] Heywood J, Rannacher R, Turek S. Artifical boundaries and flux and pressure conditions for the incompressible Navier–Stokes equations. Int J Numer Meth Flu 1996;22:325.
[17] de Leval MR, Dubini G, Migliavacca F, Jalali H, Camporini G, Redington A, Pietrabissa R. Surgery for congenital heart disease. J Thorac Cardiovas Surg 1996;111(3):502.
[18] Legendre R. Séparation de courant léconlment laminaire tridimensional. Rech Aéro 1956;54:3.